Chinese Chemical Letters 34 (2023) 107539

Contents lists available at ScienceDirect

Chinese Chemical Letters

journal homepage: www.elsevier.com/locate/cclet

Lead-free bilayer heterometallic halide perovskite with reversible phase transition and photoluminescence properties

Qiangqiang Jia[a], Ting Shao[a], Liang Tong[c], Changyuan Su[b,*], Dawei Fu[a,b,**], Haifeng Lu[a,*]

[a] Institute for Science and Applications of Molecular Ferroelectrics, Key Laboratory of the Ministry of Education for Advanced Catalysis Materials, Zhejiang Normal University, Jinhua 321004, China
[b] Ordered Matter Science Research Center, Jiangsu Key Laboratory for Science and Applications of Molecular Ferroelectrics, Southeast University, Nanjing 211189, China
[c] School of Environment and Chemical Engineering, Jiangsu University of Science and Technology, Zhenjiang 212002, China

ARTICLE INFO

Article history:
Received 17 April 2022
Revised 11 May 2022
Accepted 17 May 2022
Available online 20 May 2022

Keywords:
Lead-free
Heterometallic
Perovskite
Phase transition
Photoluminescence

ABSTRACT

The layered heterometallic halide perovskites, as a newly explored material, have attracted great scientific attention. As one of the representatives of perovskite, lead-free or lead-substituted perovskite materials are widely applied in photovoltaic, sensors, catalysis, detectors and other fields. Therefore, it is urgent to carry out more systematic exploration and expand applicable preresearch, so as to make more interesting discoveries in this new hot spot. As an interesting candidate, heterometallic compounds will introduce more structural adjustability and novel physical properties, which is the main feature to be selected as the research hotspot. Here, we reported a lead-free bilayer heterometallic Ruddlesden-Popper (RP) type perovskite, [$(MACH)_2CsAgBiBr_7$] (MACH = cyclohexanemethylamine), which possesses a reversible phase transition at 379.6 K/375.1 K during heating-cooling cycle. Besides, it exhibits reddish-brown light emission under 365 nm, meanwhile, CIE chromaticity coordinate is (0.32, 0.45) on the yellow side and correlated color temperature is about 6000 K. Moreover, both the experimental data and theoretical calculation results suggest that [$(MACH)_2CsAgBiBr_7$] shows indirect semiconducting characteristics. In summary, this work will inspire the design of lead-free heterometallic perovskite materials for the application of sensors and light-emitting diodes (LEDs) fields.

Two-dimensional (2D) layered organic-inorganic halide perovskites [1–16] (OIHPs) have swept across many areas of the scientific, such as dielectric [17–23], piezoelectric [24–30], ferroelectricity [31–39], light-emitting diodes (LEDs) [40–47], photovoltaic and photodetector. As a typical representative of lead-based perovskites, $MAPbI_3$'s excellent properties stem from its stable structure, tunable band gap, high absorption coefficient, strong carriers and other outstanding physical properties. However, the disadvantages of high toxicity and unfriendly environment limit the development of lead-based perovskite materials [16,48–51], which are mainly manifested in the harm to human body, animals and plants, and the destruction of the environment. Therefore, lead-free or lead-substituted perovskite materials have been rapidly developed.

Based on lead-based perovskites, currently, a large number of lead-free perovskites [3,52] have been reported for their structural characteristics. Particularly, Ruddlesden-Popper (RP) type perovskites with the general formula ($A_2'A_{n-1}M_nX_{3n+1}$) is one of the most advantageous candidates, in which A is monovalent cation (Cs^+, formamidine (FA), methylamine (MA), dimethylamine (DMA) and so on), A′ is organic amine cations (interlayer cations). Moreover, there is also equally important Dion-Jacobson (DJ) phase ($A'A_{n-1}M_nX_{3n+1}$) with divalent cations at A′-site. For example, Luo's group reported a bilayered two-dimensional hybrid perovskite, $(IA)_2(DMA)Pb_2Br_7$ (RP type, IA^+ = isoamy-lammonium and DMA^+ = dimethylammonium) [10], which possesses a cage-templated secondary cation, and it exhibits high efficiency photodetection property. Moreover, Zhang's group reported a DJ-type lead-free halide double perovskite, [$(3AMPY)_2AgBiI_8 \cdot H_2O$] (3AMPY = 3-(aminomethyl)pyridinium) [53], with an attractive narrow band gap of 1.86 eV and stable structure. However, the above compounds reported only possess single property, and this will make the potential applications to be limited. Therefore, design

* Corresponding authors.
** Corresponding author at: Institute for Science and Applications of Molecular Ferroelectrics, Key Laboratory of the Ministry of Education for Advanced Catalysis Materials, Zhejiang Normal University, Jinhua 321004, China.
E-mail addresses: ScyWmy@163.com (C. Su), dawei@zjnu.edu.cn (D. Fu), luhaifeng@zjnu.edu.cn (H. Lu).

https://doi.org/10.1016/j.cclet.2022.05.053
1001-8417/

and synthesis have become significant links in the exploration of multifunctional materials.

Herein, a new RP-type lead-free bilayer heterometallic halide perovskite, $[(MACH)_2CsAgBiBr_7]$ (MACH = cyclohexanemethylamine), was successfully synthesized. Differential scanning calorimetry (DSC) shows that a reversible phase transition occurs at 379.6 K, meanwhile, a dielectric responsive of the compound also exhibits at about the same temperature. Moreover, the compound possesses a charming reddish brown light emission under 365 nm lamp. Based on above properties, an important contribution of this work might provide new perspective for designing and synthesizing of lead-free multifunctional materials.

Cs_2CO_3 (98%, Bide-Shanghai), Ag_2O (99.7%, Alading-Shanghai), Bi_2O_3 (99.9%, Meryer-Shanghai), hydrobromic acid (40 wt% in water, Amethyst) and cyclohexanemethylamine (98%, Mreda-Beijing) were purchased by commercial channel and used without further purification.

Single crystals of $[(MACH)_2CsAgBiBr_7]$ were collected by cooling slowly of saturated solution. Mixture of Cs_2CO_3, Ag_2O, Bi_2O_3 and cyclohexanemethylamine with the molar ratio of 1:1:1:2. Then, adding hydrobromic acid (20 mL) to the mixture and heating until all dissolve under stirring. Orange block single crystals were obtained *via* cooling slowly (1 K/day). The final yield is about 35% (Based on organic).

The structure of the title single crystal was characterized by single crystal X-ray diffraction (SC-XRD, Bruker D8 SPEX-III) with equipping a Mo Kα radiation ($\lambda = 0.71073$ Å) at request temperature. The differential scanning calorimetry (DSC) curves was recorded on a NETZSCH DSC 2500 equipment with heating/cooling rate is 20 K/min under nitrogen atmosphere, and dielectric constant of temperature dependence were tested on Tonghui instrument under different frequencies. The solid UV-NIR-vis (UV-near-Infrared-visible light) spectrum were measured on Agilent Cary 5000 spectrometer at room temperature. The solid-state fluorescences emission spectrum was test on Agilent Cary FLS 980 instruments. The CIE coordination was calculated by 1931 CIE package. Band structure and density of state of the title compound were calculated based on structural film CIF by VASP software with density functional theory (DFT). Hirshfeld surface and 2D fingerprint were generated by CrystalExplorer package with HF functional.

Crystallographic data of the title compound were restored by SPEX-III software, and absorption was corrected by multi-scan (ω) mothed. Furthermore, the crystal structure factors were solved by least squares. Meanwhile, structural factors were refined by SHLXT and OLEX 1.2 software, and non-hydrogen atom are refined and positioned by operation of anisotropy. The figures of the title compound were carried out by DIAMOND package. Lastly, all detail parameters of three phases crystal structure were listed in the associated crystallographic information in Table S1 (Supporting information).

To further understand the phase transition-induced structural changes, single crystal X-ray diffraction (SC-XRD) of the $[(MACH)_2CsAgBiBr_7]$ were characteristic at 300 K and 385 K, respectively. Normally, the phase is named as low temperature phase (LTP) that is below the phase transition point, conversely, the high temperature phase (HTP) is considered to be the phase that is above phase transition point. Interestingly, the LTP and HTP structure of $[(MACH)_2CsAgBiBr_7]$ both crystallized in orthorhombic system. However, LTP architecture (Fig. 1a) grown in centrosymmetric (CS) chiral $P2_12_12_1$ space group (No. 19, *222* point group) with $a = 8.029(2)$ Å, $b = 8.158(2)$ Å and $c = 44.535(9)$ Å. According to the structural characteristics, $[(MACH)_2CsAgBiBr_7]$ belongs to Ruddlesden-Popper (RP) type perovskites with general formula ($A_2'A_{n-1}M_nX_{3n+1}$), which A′ is cyclohexanemethylamine cation ($HMACH^+$), and A represents Cs^+ ion, M are Ag^+ and Bi^{3+} ions,

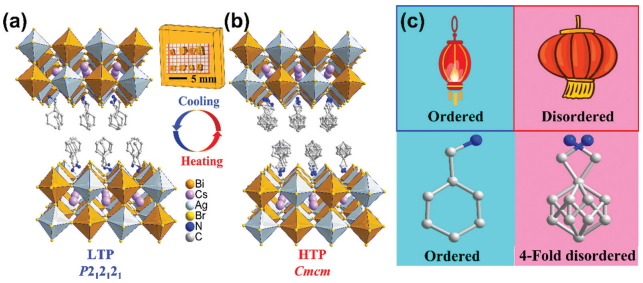

Fig. 1. Stacked structure of (a) $[(MACH)_2CsAgBiBr_7]$ at LTP (300 K) and (b) HTP (385 K). (c) Organic cation state at LTP (300 K) and HTP (385 K). Insert: Topography and physical map of single crystal.

respectively, X is Br^-. Bilayer inorganic frameworks with bimetals are crossed by octahedra in a slightly twisted configuration $[BiBr_6]^{4-}$ and $[AgBr_6]^{4-}$, [54], respectively. Meanwhile, the "perovskitizer" Cs^+ cations are located in the center of the cage-like structure of the inorganic framework, neatly aligned twisted octahedra ($[BiBr_6]^{4-}$ and $[AgBr_6]^{4-}$) and perovskite mineralizers (Cs^+) together build 2D/3D structures of inorganic frameworks. However, the slightly twisted octahedron makes the inorganic framework a tortuous plane, parts of bond lengths and bond angles are labeled in Fig. S1 (Supporting information). In addition, organic amine cations are ordered, which like an unexpanded lantern, and organic cations embedded in open cavities of $[BiBr_6]^{4-}$ and $[AgBr_6]^{4-}$ *via* hydrogen bonding (N-H···Br) and van der Waals forces. With the temperature rising above 380 K, HTP structure (Fig. 1b) of $[(MACH)_2CsAgBiBr_7]$ crystallize in *Cmcm* (No. 63, mmm point group) with $a = 8.137(2)$ Å, $b = 45.096(11)$ Å, $c = 8.1359(18)$ Å. Obviously, inorganic frameworks of bimetallic bilayers vary from tortuous planar to fully planar structures, meanwhile, the spatial coordinates of the Cs^+ ions as perovskite are not shifted. Notably, accompanying the phase transitions, strong symmetry restoring appears in HTP structure with chirality disruption along the [001] direction. Meanwhile, the transition of organic cations (Fig. 1c) from an ordered structure to a 4-fold disordered structure is accompanied by the phase transition occurring, which 4-fold disordered organic amine cations like spinning lantern. According to Fig. S3 (Supporting information), despite the different morphologies of the ligands in the high-temperature phase structure (the reason is that the positions of two organic ligands with different morphologies are different from the relative positions of the symmetry operation planes), the occupancy rate of all carbon atoms is 0.25, and the occupancy rate of nitrogen atoms also are 0.25. In addition, symmetric operations (Fig. S2 in Supporting information) are also increased from [*E, C2, 2C2′*] (LTP) to [*E, C2, 2C2′, i, 3σ*] (HTP). Parts of important bong lengths and bond angles are listed in Table S2 (Supporting information).

To investigate the process of reversible structural phase transition of the title compound, DSC and dielectric contant (ε', Fig. 2a) of $[(MACH)_2CsAgBiBr_7]$ was executed under nitrogen atmosphere. The results indicate (Fig. 2b) that a pair of distinct thermal anomalous peaks are observed at 379.6 K and 375.1 K under heating and cooling process, respectively, and a thermal hysteresis of 4.5 K can preliminarily determine that the compound has undergone a first-order phase transition process. Meanwhile, the corresponding entropy changes (ΔS) for $[(MACH)_2CsAgBiBr_7]$ is calculated as 4.79 J K^{-1} mol^{-1} during the phase transition. Moreover, dielectric constant of temperature dependence was also performed (Fig. 2c, 1 MHz) that two obvious dielectric anomalies are found at about 380 K during heating and cooling process (this is in agreement with the DSC, further confirming the occurrence of a temperature-triggered reversible phase transition), and the value of real part (ε') dielectric constant increases gradually with the increase of

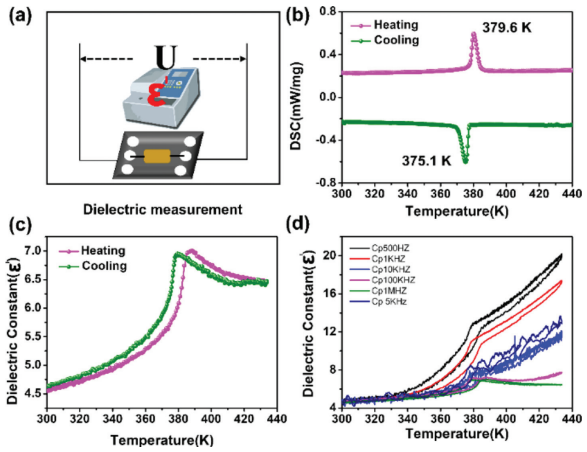

Fig. 2. (a) Schematic diagram of dielectric test of polycrystalline tablet. (b) DSC curves of the $[(MACH)_2CsAgBiBr_7]$. (c) The value of real part (ε') dielectric constant under 1 MHz. (d) The dielectric constant of frequency dependence under different frequency.

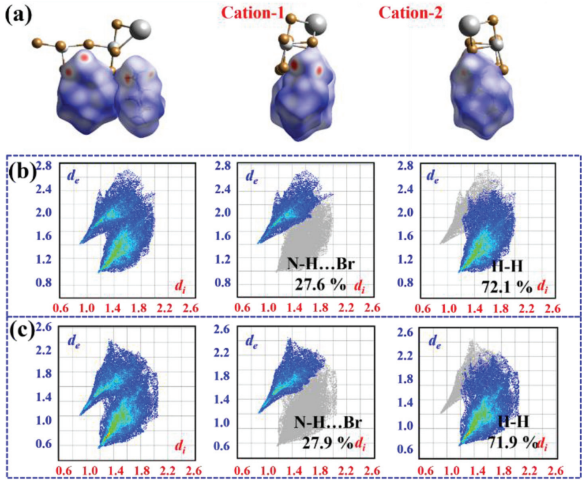

Fig. 3. Hirshfeld surface and related 2D fingerprint plot of $[(MACH)_2CsAgBiBr_7]$. (a) Hirshfeld surface of two cations in LTP cell. (b) Related 2D fingerprint plot of cation-1. (c) Related 2D fingerprint plot of cation-2.

temperature from *ca.* 4.5 to *ca.* 7.0 below 380 K, and a step-like jump of dielectric constant appears when temperature is up to 380 K. Thereafter, the value of ε' gradually decreases and plateaus. Meanwhile, dielectric constant of frequency dependence (500 Hz, 1 kHz, 5 kHz, 10 kHz and 100 kHz) were also recorded (Fig. 2d) that the dielectric constant has the same increasing trend at different frequencies, and the value of the dielectric constant increases with decreasing frequency about from 4 to 20. What is more, the dielectric cycles of $[(MACH)_2CsAgBiBr_7]$ was measured at 1 kHz. As shown in Fig. S4 (Supporting information) that the dielectric constant of $[(MACH)_2CsAgBiBr_7]$ can maintain the stability after heating-cooling dielectric cycles of high-low state switching (*ca.* 18 and 4, respectively). Thus, the stable dielectric cycling suggests this compound may be a potential thermal sensors and switches. Therefore, the $[(MACH)_2CsAgBiBr_7]$ might be a potential dielectric responsive material.

To further investigate the change of weak force during the phase transition of the compound, Hirshfeld surface and related 2D fingerprint plot were generated based on CIF files (LTP) with structure factors by CrystalExplorer program using HF functional theory. As shown in Fig. 3a, the forces of the two organic amine cations are slightly different in the minimal asymmetric unit, the red regions represent relatively strong interactions between different asymmetric units, which induces the directional orientation of single molecule (such as two cations in the LTP cell). The intermolecular interactions between bromine atom and H on the cyclohexanemethylamine were demonstrated in the Hirshfeld surface as the red areas in Fig. 3a, and the bright red spots are corresponding to C-H···Br interactions, and the Br···H-N/N-H···Br intermolecular interactions appear as distinct spikes in the 2D fingerprint plot (Figs. 3b and c). The proportion of Br···H-N/N-H···Br interactions comprises 27.6% and 27.9% of the total Hirshfeld surface, respectively, which shows the strong interactions are mainly contributed by C-H···Br, confirming the critical role of the synergistic effect of organic and inorganic components. From the Hirshfeld surface analysis, the results are well consistent with the single-crystal structure determinations.

As demonstrated in Fig. 4a, the orange polycrystalline powder of $[(MACH)_2CsAgBiBr_7]$ possess reddish-brown emission under 365 nm lamp. Furthermore, solid-state photoluminescence (PL) spectroscopy (Fig. 4b) of the compound is characterized at room temperature, the results indicate that the maximum excitation wavelength is 369 nm, and the corresponding maximum emission wavelength is 522 nm, meanwhile, a weaker emission peak appears at 647 nm, and the Stokes shifts corresponding to the two emission peaks are 153 nm and 278 nm, respectively. According to the compounds with similar structure reported in the literature [55–57], the photoluminescence effect of the compound is attributed to the quantum confinement effect caused by the twisted octahedral structure, electronic transitions at the top of the valence band. As shown in Fig. 4c, the CIE chromaticity coordinates (1931) of the compound are calculated and drawn to be (0.32, 0.45), which is located on the yellow side, and correlated color temperature is about 6000 K. Moreover, PL decay time (Fig. 4d) was measured that the resulting lifetime (τ) was obtained and calculated as 4.06 ns. Thus, this material might be a potential candidate in the light-emitting diodes (LEDs) field.

To understand the semiconducting properties of $[(MACH)_2CsAgBiBr_7]$, optical UV-NIR-vis absorption spectrum was performed. The results reveal that the maximum relatively sharp absorption edge reaches approximately 600 nm, suggesting indirect band gap semiconductor. The optical band gap (Fig. S5 in Supporting information) was calculated as 2.08 eV by the *Tauc* equation $(h\nu \cdot F(R_\infty))^{1/n} = A(h\nu - E_g)$ [58]. Moreover, the band structure, correlated density of states (DOS) and theoretical band gap of $[(MACH)_2CsAgBiBr_7]$ was also calculated based on structural film CIF by VASP software with density functional theory (DFT). The calculation results show that the relative positions of the valence band maximum (VBM,) and the conduction band minimum (CBM) in space are misaligned, which $[(MACH)_2CsAgBiBr_7]$ can be further identified as indirect bandgap semiconductor. Meanwhile, the theoretical band gap was also considered as 1.991 eV. In addition, the correlated density of states (DOS) was also recorded, it shows that the valence band maximum (VBM) and conduction band minimum (CBM) of the compound are mainly contributed by the inorganic network part (Ag-s, Ag-p, Ag-d, Bi-s, Bi-p, Bi-d and Br-s, Br-p), moreover, H-s, C-p and N-p states widely overlap in organic section, suggesting a strong interaction. What's more, the results of partial density of state (PDOS, Fig. S6a in Supporting information) further suggest that the conduction band was contributed by Ag-sp, Bi-sp and a little Cs-sp, and the valence band was mainly formed by Br-sp, C-sp, H-s and a little N-sp. As demonstrated in Fig. S6b (Supporting information) that frontier molecular orbitals (FMO-HOMO and LUMO) of $[(MACH)_2CsAgBiBr_7]$ are located in inorganic framework part, thus, the FMO indirect prove that the energy band was contributed by inorganic skeleton. The compound is an outstanding indirect narrow bandgap semiconductor with band gap as 2.08 eV. Therefore, it may show potential photo-

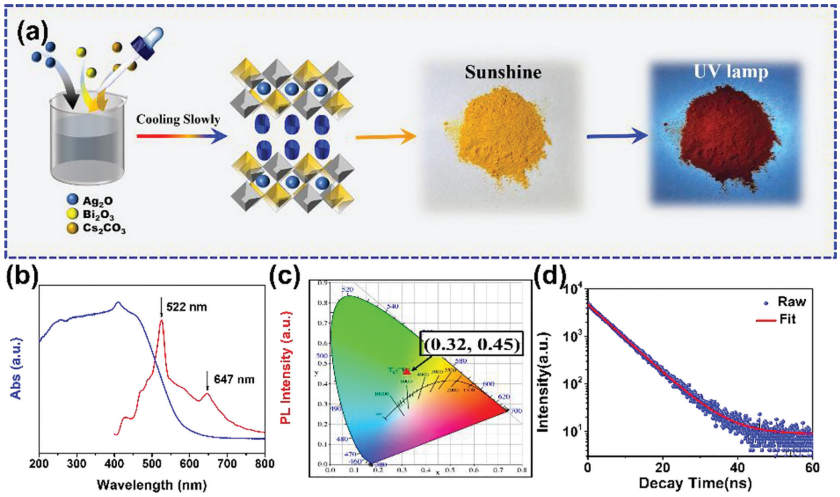

Fig. 4. (a) Synthesis process schematic of $[(MACH)_2CsAgBiBr_7]$ and photoluminescence physical map. (b) UV absorption and photoluminescence emission spectra. (c) CIE chromaticity coordinates (1931) of $[(MACH)_2CsAgBiBr_7]$. (d) PL decay time of $[(MACH)_2CsAgBiBr_7]$.

voltaic characteristics and provide new candidates in subsequent exploration [59,60].

In summary, a new lead-free bilayer bimetallic Ruddlesden-Popper (RP) type perovskite, $[(MACH)_2CsAgBiBr_7]$ (MACH = cyclohexanemethylamine), was successfully synthesized *via* cooling slowly of saturated solution, and large-sized single crystals are obtained by the apical growth method. The compound exhibits a reversible phase transition at 379.6 K/ 375.1 K during heating and cooling, therefore, the dielectric switching was clearly indicated by the steady-state switchable dielectric cycling. Meanwhile, it displays a reddish-brown light emission under ultraviolet light, and CIE coordinate of $[(MACH)_2CsAgBiBr_7]$ is (0.32, 0.45), moreover, the correlated color temperature is about 6000 K. In addition, both the experimental data and theoretical calculation results suggest that $[(MACH)_2CsAgBiBr_7]$ shows indirect semiconducting characteristics. Moreover, thermogravimetric analysis (TGA) of the compound shows that the material possesses good thermal stability of chemical structure. In short, this compound might be a potential candidate in sensors, dielectric responsive, light-emitting diodes (LEDs) and semiconductors fields. This work might provide a new perspective for designing of lead-free metal-halide perovskite materials.

Declaration of competing interest

The authors declare that they have no known competing financial interests or personal relationships that could have appeared to influence the work reported in this paper.

Acknowledgments

This work was supported by the National Natural Science Foundation of China (No. 21991141), and Zhejiang Normal University.

Supplementary materials

The supplementary crystallographic data for this paper has been uploaded in the Cambridge Structural Database. The number of CCDC are as follows: 2166649 (LTP) and 2166650 (HTP). Supplementary material associated with this article can be found, in the online version, at doi:10.1016/j.cclet.2022.05.053.

References

[1] Y. Ma, J. Wang, W. Guo, et al., Adv. Funct. Mater. 31 (2021) 2103012.
[2] C. Shi, L. Ye, Z.X. Gong, et al., J. Am. Chem. Soc. 142 (2020) 545–551.
[3] C. Su, M. Lun, Y. Chen, et al., CCS Chem. (2021) 2021–2031.
[4] F. Jiang, H. Peng, C. Li, et al., Chin. Chem. Lett. 3 (2020) 801–804.
[5] B. Wang, H. Chen, W. Guo, et al., J. Mater. Chem. C 9 (2021) 17349–17356.
[6] C. Zhang, T. Li, L. Pu, et al., Chin. Chem. Lett. 9 (2020) 2499–2502.
[7] H.Y. Zhang, Z.X. Zhang, X.J. Song, et al., J. Am. Chem. Soc. 142 (2020) 20208–20215.
[8] H.Y. Zhang, X.J. Song, X.G. Chen, et al., J. Am. Chem. Soc. 142 (2020) 4925–4931.
[9] W. Zhang, M. Hong, J. Luo, Angew. Chem. Int. Ed. 59 (2020) 9305–9308.
[10] L. Tang, H. Chen, Y. Ma, et al., Inorg. Chem. Front. 9 (2022) 637–644.
[11] J. Zhou, L. Ding, F. Zhao, et al., Chin. Chem. Lett. 2 (2020) 554–558.
[12] X.L. Xu, L.B. Xiao, J. Zhao, et al., Angew. Chem. Int. Ed. 59 (2020) 19974–19982.
[13] W.Y. Zhang, Y.Y. Tang, P.F. Li, et al., J. Am. Chem. Soc. 139 (2017) 10897–10902.
[14] Y. Zhang, H.Y. Ye, H.L. Cai, et al., Adv. Mater. 26 (2014) 4515–4520.
[15] W. Xu, M. Niu, X. Yang, et al., Chin. Chem. Lett. 32 (2021) 489–492.
[16] Y.Y. Tang, Y. Xie, Y.L. Zeng, et al., Adv. Mater. 32 (2020) 2003530.
[17] Z.X. Zhang, C.Y. Su, J. Li, et al., Chem. Mater. 33 (2021) 5790–5799.
[18] G. Zhou, J. Ding, X. Jiang, et al., J. Mater. Chem. C 10 (2022) 2095–2102.
[19] S. Liu, L. He, Y. Wang, et al., Chin. Chem. Lett. 33 (2022) 1032–1036.
[20] S.Y. Zhang, X. Shu, Y. Zeng, et al., Nat. Commun. 11 (2020) 2752.
[21] L. Zhou, R.X. Li, P.P. Shi, et al., Inorg. Chem. 59 (2020) 18174–18180.
[22] C. Zhang, T. Li, L. Pu, et al., Chin. Chem. Lett. 31 (2020) 2499–2502.
[23] Y. Sun, W. Chen, Z. Sun, Chin. Chem. Lett. 33 (2022) 1772–1778.
[24] L. Chen, W.Q. Liao, Y. Ai, et al., J. Am. Chem. Soc. 142 (2020) 6236–6243.
[25] X.X. Chen, D.X. Liu, Y.P. Gong, et al., Inorg. Chem. 61 (2022) 2219–2226.
[26] H.Y. Liu, H.Y. Zhang, X.G. Chen, et al., J. Am. Chem. Soc. 142 (2020) 15205–15218.
[27] Q.R. Meng, W.J. Xu, W.H. Hu, et al., Chem. Commun. 57 (2021) 6292–6295.
[28] H.Y. Zhang, X.G. Chen, Y.Y. Tang, et al., Chem. Soc. Rev. 50 (2021) 8248–8278.
[29] C. Shi, J.J. Ma, J.Y. Jiang, et al., J. Am. Chem. Soc. 142 (2020) 9634–9641.
[30] Z.X. Zhang, H.Y. Zhang, W. Zhang, et al., J. Am. Chem. Soc. 142 (2020) 17787–17794.
[31] X.X. Chen, X.Y. Zhang, D.X. Liu, et al., Chem. Sci. 12 (2021) 8713–8721.
[32] S.N. Cheng, K. Ding, T. Zhang, et al., Chemistry 27 (2021) 17655–17659.
[33] D.W. Fu, J.X. Gao, W.H. He, et al., Angew. Chem. Int. Ed. 59 (2020) 17477–17481.
[34] D.W. Fu, J.X. Gao, P.Z. Huang, et al., Angew. Chem. Int. Ed. 60 (2021) 8198–8202.
[35] S. Han, M. Li, Y. Liu, et al., Nat. Commun. 12 (2021) 284.
[36] Y. Wu, H. Jiang, S. Jiao, et al., Adv. Opt. Mater. (2021) 2101905.
[37] H.Y. Zhang, X.G. Chen, Z.X. Zhang, et al., Adv. Mater. 32 (2020) 2005213.
[38] H.Y. Zhang, X.J. Song, H. Cheng, et al., J. Am. Chem. Soc. 142 (2020) 4604–4608.
[39] H.Y. Zhang, Z.X. Zhang, X.G. Chen, et al., J. Am. Chem. Soc. 143 (2021) 1664–1672.
[40] D. Li, W. Wu, S. Wang, et al., J. Mater. Chem. C 8 (2020) 6710–6714.
[41] J.Y. Li, Q.L. Xu, S.Y. Ye, et al., Chem. Commun. 57 (2021) 943–946.
[42] T. Shao, R.Y. Ren, P.Z. Huang, et al., Dalton Trans. 51 (2022) 2005–2011.
[43] Y.Y. Tang, J.C. Liu, Y.L. Zeng, et al., J. Am. Chem. Soc. 143 (2021) 13816–13823.
[44] Y. Wang, Z. Tang, C. Liu, et al., J. Mater. Chem. C 9 (2021) 223–227.
[45] Y.L. Wei, J. Jing, C. Shi, et al., Inorg. Chem. Front. 5 (2018) 2615–2619.
[46] Y. Wu, W. Fan, Z. Gao, et al., Nano Energy 77 (2020) 105170.
[47] Z. Qi, H. Gao, X. Yang, et al., Inorg. Chem. 60 (2021) 15136–15140.
[48] N. Hoshino, T. Akutagawa, J. Chem. Phys. 153 (2020) 194503.
[49] Q.Q. Jia, Q.F. Luo, H.F. Ni, et al., J. Phys. Chem. C 126 (2022) 1552–1557.
[50] W.L. Kang, Y.T. Tsai, Y.C. Ji, et al., Chem. Eur. J. 27 (2021) 17785–17793.
[51] W.Q. Liao, Y. Zhang, C.L. Hu, et al., Nat. Commun. 6 (2015) 7338.
[52] Y. Yao, H. Jiang, Y. Peng, et al., J. Am. Chem. Soc. 143 (2021) 15900–15906.

[53] D. Fu, S. Wu, Y. Liu, et al., Inorg. Chem. Front. 8 (2021) 3576–3580.
[54] X. Liu, Z. Xu, P. Long, et al., Chem. Mater. 32 (2020) 8965–8970.
[55] C. Ji, S. Wang, L. Li, et al., Adv. Funct. Mater. 29 (2018) 1805038.
[56] J. Li, C. Xu, W.Y. Zhang, et al., J. Mater. Chem. 8 (2020) 1953–1961.
[57] Y. Li, C. Ji, L. Li, et al., Inorg. Chem. Front. 8 (2021) 2119–2124.
[58] J. Tauc, R. Grigorov, A. Vancu, Phys. Status Solidi B 15 (1966) 627–637.
[59] T. Zhang, K. Ding, Y. Li, et al., Chin. J. Chem. 40 (2022) 1559–1565.
[60] Y. Chen, C. Gao, T. Yang, et al., Chin. J. Struct. Chem. 41 (2022) 2204001–2204011.